Modeling the Interface Dynamics in Continuous Casting Molds employing ANSYS CFX®

K. L. Z. Glitz[1], A. F. C. Silva[1], C. R. Maliska[1], R. N. Borges[2], A. B. Soprano[1], B. T. Vale[1]

[1] SINMEC – Computational Fluid Dynamics Laboratory, Department of Mechanical Engineering, Federal University of Santa Catarina, 88040-900. Florianopolis, Brazil.

[2] Magnesita Refratários S. A. Contagem-MG, Brazil.

ABSTRACT: There are some mechanisms in continuous casting that could cause the entrapment of slag. One of them is the entrapment due to the high shear stress acting on the interface between the molten steel and the slag. There are few works in the literature about the behaviour of the interface between slag and steel. These works apply experimental and numerical approaches to this problem. However, instead of slag and steel others fluids are employed. In order to evaluate the steel-slag interface dynamics, simulations of water flow in continuous casting molds are carried out employing the software ANSYS CFX® 11.0. The results are compared to experimental and numerical results published in the literature. ANSYS CFX® results presented good agreement with the experimental data.

1. Slag Entrapment in Continuous Casting Introduction

In continuous casting molten steel is injected into the mold through a submerged entry nozzle (SEN). The molten steel flows from the SEN, reaches the narrow face of the mold and then flows towards the SEN again, causing shear stress on the interface. Depending on the superficial velocity of the molten steel near the slag-steel interface, slag can be entrained into the steel bath [4]. This entrapment of slag results in a defect in the final product and must be avoided. Therefore it is of fundamental importance to determine the critical value of the superficial velocity of steel beyond which slag is entrained.

In the literature there are few works about the behaviour of the interface between slag and steel. These works apply experimental and numerical approaches to this problem. However, instead of slag and steel, other fluids are employed. For the case of silicon oil and water flow, it is related that the critical superficial velocity of water beyond which silicon oil is entrained in the water bath lies between 0.15 and 0.4 m/s [5,6].

One of such works employing different fluids was done by Gupta and Lahiri [3]. They studied experimentally the water flow inside casting molds with different aspect ratios. Employing different port diameters and angles, they analysed the effect of the casting-speed in the meniscus behaviour. In their paper there are five consecutive frames showing the interface position at different times, with an interval of 0.04 s among them. One of these pictures shows the entrapment of a bubble.

Based on the work of Gupta and Lahiri, Dash and coworkers [2] performed two-dimensional numerical simulations of the water flow in a mold. Their objective was to predict the shape of the free surface and the entrapment of air bubbles. They compared their numerical results with those obtained by Gupta and Lahiri in their experiments, and concluded that their results presented good agreement with the experimental ones.

In this work, numerical simulations of the water flow in 1:8 aspect ratio mold of [3] were carried out employing the software ANSYS CFX® 11.0. The results obtained in these simulations were compared to those obtained numerically by [2] and experimentally by [3], and will be presented further.

2. Experimental Model

In their study, Gupta and Lahiri employed a 80 mm-thickness mold and a SEN with parallel ports. The submergence depth was kept at 150 mm. This mold is illustrated in Fig. 1, which is based on the figure presented in [2]. In this figure the shaded area indicates the portion of the domain occupied by water at time t=0.

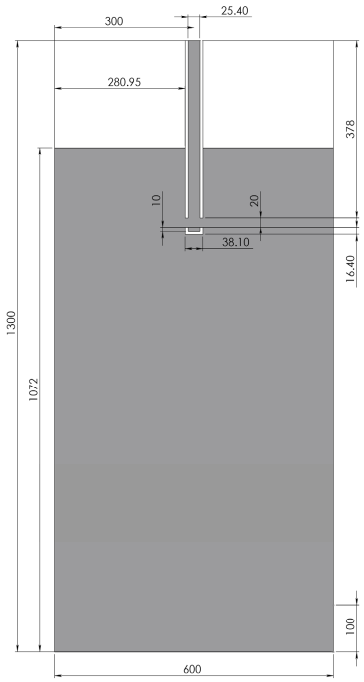

Fig. 1: The mold employed in the experiments by [3] and in the numerical simulations (Dimensions in mm).

In the experiments the water flow rate was equal to 1.22 x 10^{-3} m^3/s.

3. NUMERICAL MODEL

As well as the numerical simulations carried out by Dash and coworkers, those employing the software ANSYS CFX® 11.0 also considered two-dimensional flow inside the mold illustrated in Fig. 1, by employing a one element thickness-grid.

Since the outlet was placed on one side of the mold's wall, the water flow could not be considered symmetric. Thus a full-scale model of the mold was employed in the simulations.

Once the water flow is turbulent and transient and the fluids (water and air) are incompressible, Newtonian and isothermal, the governing equations of this problem are:

$$\frac{\partial r_\alpha}{\partial t} + \frac{\partial}{\partial x_i}\left(r_\alpha U_i\right) = 0 \tag{1}$$

which is the equation of continuity applied to both fluids,

$$\frac{\partial \rho}{\partial t} + \frac{\partial}{\partial x_i}\left(\rho U_i\right) = 0 \tag{2}$$

which is the equation of continuity for the mixture,

$$\frac{\mathrm{D}\left(\rho U_i\right)}{\mathrm{D}t} = -\frac{\partial p}{\partial x_i} + \frac{\partial}{\partial x_j}\left[\mu\left(\frac{\partial U_i}{\partial x_j} + \frac{\partial U_j}{\partial x_i}\right) - \rho\overline{u_i u_j}\right] + \rho g_i + F_{\sigma i} \tag{3}$$

Equation (3) is the momentum equation.

In these equations r_α is the volume fraction of fluid α, $\rho\overline{u_i u_j}$ are the Reynolds stresses and F_{σ_i} is the component in direction i of the force due to surface tension. The fluid properties are functions of the volume fractions of the fluids:

$$\rho = r_1\rho_1 + (1 - r_1)\rho_2 \tag{4}$$

$$\mu = r_1\mu_1 + (1 - r_1)\mu_2 \tag{5}$$

where the subscripts 1 and 2 denote water and air, respectively.

All the numerical simulations employed the k-ε model in order to calculate the turbulence parameters. This model solves two equations: one for the turbulent kinetic energy (k) and another for the rate of dissipation of turbulent kinetic energy (ε).

The surface tension effects are included in the momentum equations as a body force. This force is obtained through the Continuum Surface Force model (CSF). In this model the effects of this force are spread across a region around the interface of variable volume fraction [1].

3.1 Properties of the Fluids

In the numerical simulations it was employed water and air. The physical properties of these two fluids are listed in Tab. 1.

	Water	Air
Density (kg/m³)	988.3	1.225
Viscosity (Pa s)	0.001013	1.8×10^{-5}
Surface tension (N/m)	0.073	

Tab. 1: Properties of the fluids.

3.2 Boundary Conditions

In order to simulate the water flow inside the mold, the following boundary conditions were employed:

- Inlet: prescribed values for the normal velocity and the turbulence intensity. Only water flows through this boundary;
- Outlet: Bulk mass flow rate equal to the mass flow rate at inlet;
- Top of the domain: prescribed value for the static pressure. At this boundary both fluids are allowed to leave the domain.

The remaining boundaries of the domain were considered to be walls with the no slip condition.

In the ANSYS CFX® simulations it was employed a 2% turbulence intensity at the inlet.

It is necessary to make some remarks about the prescribed value of the normal component of the velocity at the inlet. Dash, Mondal and Ajmani [2] reported in their work that bubble entrapment occurs at an inlet velocity of 2 m/s or more. Based on the value of the water mass flow rate mentioned by Gupta and Lahiri in their work [3], Dash et al. considered that the average port exit velocity of the experiments of [3] was equal to 1.94 m/s. According to them this value corresponds to an inlet velocity of 3 m/s in the numerical two-dimensional computation.

Thus it was considered an inlet velocity of 3 m/s in the numerical simulations performed by ANSYS CFX® 11.0.

3.3 Initial Conditions

As mentioned above the initial field of the volume fractions is the one illustrated in Fig. 1, in which the shaded area indicates the portion of the domain occupied by water. The white area between the interface and the top of the domain is filled by air. There is a smoothed transition of the values of the volume fractions across the interface, in order to avoid abrupt changes in the values of the variables.

At time t=0 the velocity field is set equal to zero, except the velocity at the inlet where the normal component of the velocity is prescribed a value equal to 3 m/s. All the turbulence parameters are also set equal to zero in the entire domain, except the value at the inlet.

3.4 Grid Size and Timestep

Dash et al. did not give detailed information about the grid that they employed. In their work there is a figure of the grid, however the only numerical information about it is the size of the cells around the interface. In that zone the cells are refined to a size of 2.5 x 2.5 mm. In their work there is also a lack of information about the timestep value employed.

In the simulations performed by ANSYS CFX® 11.0 it was employed four different

grids, each one with 43444, 85124, 141732 and 302780 nodes. Therefore a study of the dependence of the results on the grid size could be carried out. For these grids the sizes of the cells around the interface are 5.7 x 2.0 mm (in x-direction and y-direction), 3.6 x 1.4 mm, 2.2 x 1.4 mm and 1.5 x 1.3 mm respectively. This refinement is applied to a 100 mm-wide region which involves the interface at its initial position.

After carrying out a timestep depence study, it was concluded that the optimal value for the timestep is 10^{-4} s. This timestep assures a small value of the Courant number, consequently implying in realistic results.

4. RESULTS

As mentioned above simulations were performed with different grid sizes. The results of these simulations were compared to those obtained numerically by [2] and experimentally by [3].

In Fig. 2 and 3 it is shown the position of the interface relative to its initial position at two different times for the left half of the mold (Fig. 1) obtained numerically. In these figures the results obtained in the present work employing the finer grid are compared to those obtained by [2].

As can be observed the numerical results in each figure do not correspond to the same time instant. While the interface position at t=1.04 and 1.2 s obtained by ANSYS CFX® is plotted in Fig. 2 and 3 respectively, the results of [2] shown in these figures correspond to t=1.2 and 1.36 s. This is done because in the ANSYS CFX® simulations bubble entrapment occurs earlier (at approximately t=1.2 s) than in the simulations performed by Dash et al., which occurs at approximately t=1.36 s.

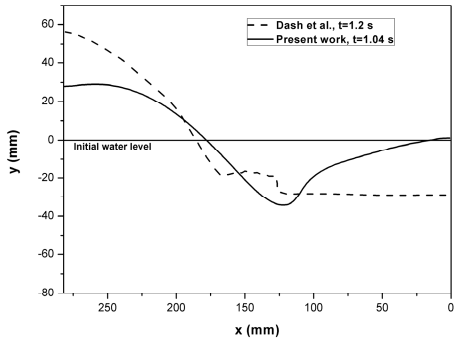

Fig. 2: Interface position at t=1.04 s (Present work) and at t=1.2 s (Dash et al.)

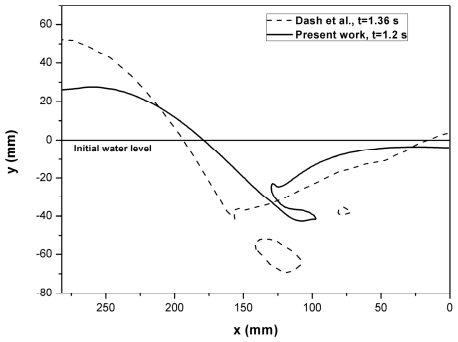

Fig. 3: Interface position at t=1.2 s (Present work) and at t=1.36 s (Dash et al.)

In both figures the position x=280.95 mm corresponds to the mold narrow side and x=0 mm corresponds to the SEN wall.

Since the exact time at which a bubble is entrapped during the experiments is not known, it is not possible to affirm which of the entrapment times obtained numerically is the correct one.

Comparing the results to those obtained by Gupta and Lahiri (Fig. 4 and 5) it can be seen that the results obtained in the present work are qualitatively and quantitatively better than those obtained by [2].

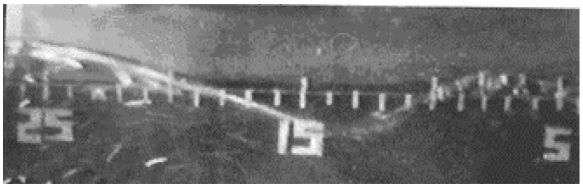

Fig. 4: Interface position obtained by Gupta and Lahiri (Fig. 7(b) of [3]).

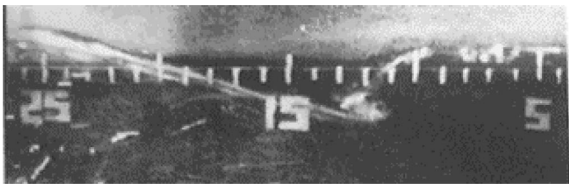

Fig. 5: Interface position obtained by Gupta and Lahiri at 0.08 s after Fig. 4.

As can be observed in Fig. 2 and 3, the wave amplitude of the interface near the SEN

wall obtained in the present work is higher than the wave amplitude obtained by Dash et al., differing from the amplitude of the experiments in only a few millimetres.

Also the shape of the interface before the breakup presented in this paper shows good agreement to the experimental results.

4.1 Grid Independence Results

Dash et al. performed a study on the influence of the grid size on the numerical results for the position of the interface. Besides the grid with 2.5 x 2.5 mm cells around the interface, they also employed a refined grid whose cells' size around the interface was equal to 1.25 x 1.25 mm. They concluded that the coarser grid was able to reproduce satisfactorily the experimental results.

In the present work four grids with different refinement levels were employed in the simulations. The position of the interface at t=1.04 s obtained employing these grids is shown in Fig. 6.

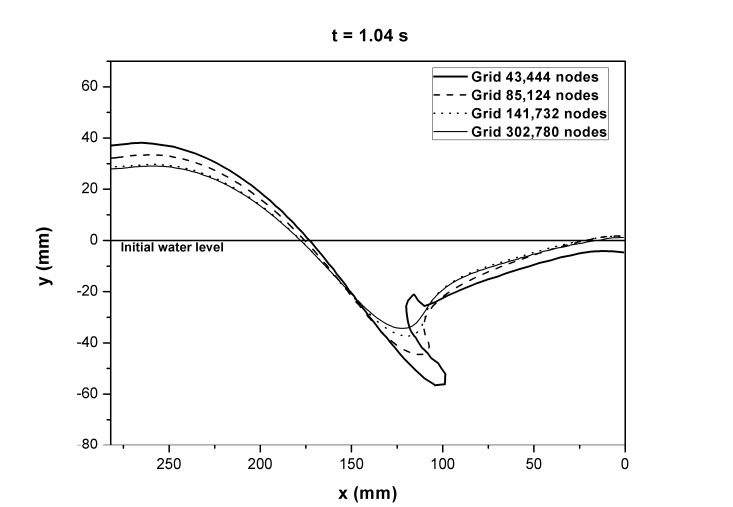

Fig. 6: Interface position along the mold width at t=1.04 s for four different grids.

As can be seen in this figure there is a considerable difference between the results for the coarsest and the finest grids. The coarser the grid employed, earlier is the breakup of the interface.

Despite some little difference it can be concluded that the results obtained employing the grid with 141732 nodes (2.2 x 1.4 mm cells around the interface) are quite similar to those obtained when the finest grid was employed.

4.2 Surface Tension

Simulations neglecting the effects of the surface tension were performed too. As their results were very similar to those obtained considering these effects, it can be concluded that surface tension plays no important role in this problem.

4.3 Superficial Velocity of Water near the Interface

Since one of the most important parameters of flow related to the slag entrapment problem is the superficial velocity of the molten steel near the interface, some results for this parameter for the water flow along the mold's width are presented below.

The Fig. 7 and Fig. 8 illustrate the behaviour of the horizontal component of the superficial velocity of water near the interface at t=1.16 and 1.2 s. At this time instant the entrapment of a bubble is imminent. These figures were built by considering a contour of the volume fraction of water equal to 99 %.

As can be seen in these figures the superficial velocity of water before the breakup is higher than that observed when the interface break-up is about to happen. At t=1.16 s the maximum value of this velocity is around 0.86 m/s and after 0.04 s it is equal to 0.83 m/s. The maximum values of the superficial velocity of water occur at the through of the wave at the interface.

Thus the critical value of the water superficial velocity beyond which air is entrapped is around 0.86 m/s.

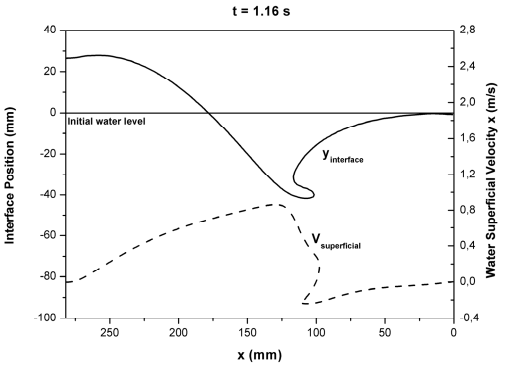

Fig. 7: Interface position and water superficial velocity at t=1.16 s.

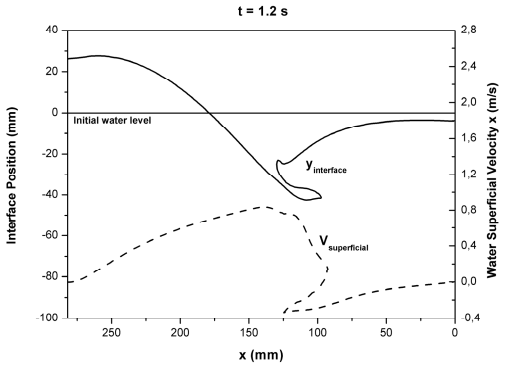

Fig. 8: Interface position and water superficial velocity at t=1.2 s.

5. CONCLUSIONS

As shown in the previous section the numerical results obtained by employing the software ANSYS CFX® 11.0 showed better agreement to the experimental ones than those obtained numerically by Dash and coworkers [2].

It was also concluded in this work that surface tension plays no important role in the entrapment of bubbles by water flow.

An important contribution of this work is the establishment of numerical values for the critical superficial velocity of water beyond which air is entrapped in the water bath.

6. ACKNOWLEDGMENTS

The authors would like to express their gratitude to FINEP and to Magnesita Refratários S.A. for sponsoring this research project. The first author would also like to express her gratitude to the National Council for Scientific and Technological Development (CNPq) for sponsoring her doctorate study.

7. BIBLIOGRAPHIES

[1] Brackbill, J.; Kothe, D.; Zemach, C.: A Continuum Method for Modeling Surface Tension, Journal of Computation Physics, v. 100 (1992), pp. 335-354.

[2] Dash, S.; Mondal, S.; Ajmani, S.: Mathematical simulation of surface wave created in a mold due to submerged entry nozzle, International Journal of Numerical Methods for Heat and Fluid Flow, v. 14 (2004), pp. 606-632.

[3] Gupta, D.; Lahiri, A.: Water-Modeling Study of the Surface Disturbances in Continuous Slab Caster, Metallurgical and Materials Transactions B, v. 25B (1994), pp. 227-233.

[4] Iguchi, M.; Yoshida, J.; Shimizu, T.; Mizuno, Y.: Model Study on the Entrapment of Mold Powder into Molten Steel, ISIJ International, v. 40 (2000), pp. 685-691.

[5] Suzuki, M.; Suzuki, M.; Nakada, M.: Perspectives of Research on High-speed Conventional Slab Continuous Casting of Carbon Steels, ISIJ International, v. 41 (2001), pp. 670-682.

[6] Thomas, B.: Fluid Flow in the Mold. Making, Shaping and Treating of Steel, The AISE Steel Foundation (2003).